Report

Cell Reports

The N Terminus of the OB Domain of Telomere Protein TPP1 Is Critical for Telomerase Action

Graphical Abstract

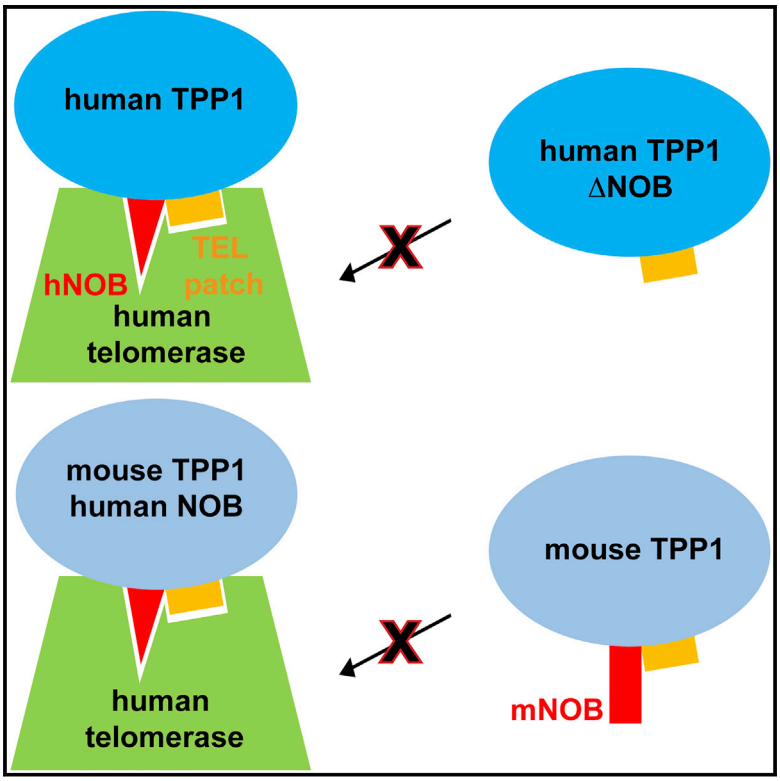

Authors

Sherilyn Grill, Valerie M. Tesmer, Jayakrishnan Nandakumar

Correspondence

jknanda@umich.edu

In Brief

TPP1 protein is critical for telomerase function and telomere length maintenance. Grill et al. find that the TPP1 NOB region is part of the surface that mediates these functions. The inability of mouse TPP1 to stimulate human telomerase is partially rescued by swapping in the human NOB sequence.

Highlights

- TPP1 NOB is critical for telomerase processivity and recruitment to telomeres
- Deletion of TPP1 NOB results in telomere shortening in cultured human cells
- Function of TPP1 NOB does not rely on binding to POT1 or TIN2
- Human TPP1 NOB sequence enables mouse TPP1 to stimulate human telomerase

Grill et al., 2018, Cell Reports *22*, 1132–1140
January 30, 2018 © 2018 The Author(s).
https://doi.org/10.1016/j.celrep.2018.01.012

CellPress

OPEN ACCESS
CellPress

Cell Reports
Report

The N Terminus of the OB Domain of Telomere Protein TPP1 Is Critical for Telomerase Action

Sherilyn Grill,[1,2] Valerie M. Tesmer,[1,2] and Jayakrishnan Nandakumar[1,3,*]
[1]Department of Molecular, Cellular, and Developmental Biology, University of Michigan, Ann Arbor, MI 48109, USA
[2]These authors contributed equally
[3]Lead Contact
*Correspondence: jknanda@umich.edu
https://doi.org/10.1016/j.celrep.2018.01.012

SUMMARY

Telomerase recruitment to telomeres and enzymatic processivity are mediated by TPP1, an essential component of telomere integrity and telomerase function. A surface on the OB domain of TPP1 called the TEL patch is critical for TPP1's telomerase-associated functions. Here, we identify a separate region in the N terminus of the OB domain (termed NOB) of TPP1 that, like the TEL patch, is essential for telomerase repeat addition processivity *in vitro* as well as telomerase recruitment to telomeres and telomere lengthening in cells. Although well-conserved among most mammalian TPP1 homologs, the NOB region in mice is distinct. Swapping the sequence of human NOB into mouse TPP1 allows it to stimulate human telomerase, qualifying NOB as an important determinant of species specificity for TPP1-telomerase interaction. Our studies show that TPP1 NOB is critical for telomerase function and demonstrate that the telomerase interaction surface on TPP1 is more elaborate than previously appreciated.

INTRODUCTION

In most eukaryotes, continued cell division is made possible through activation of the ribonucleoprotein (RNP) enzyme telomerase (Hahn et al., 1999). Telomerase compensates for the shortening of chromosomes that occurs during DNA replication by synthesizing the telomeric repeat sequence (GGTTAG in humans) at chromosome ends (Greider and Blackburn, 1985). This process is essential for stem cell renewal (Shay and Wright, 2010), and mutations that negatively impact telomerase function result in inheritable telomeropathies, such as dyskeratosis congenita (Dokal, 2011; Savage, 2014). Telomerase is also responsible for conferring replicative immortality in ~90% of all known cancers, qualifying it as a prime target for anti-cancer drug development (Kim et al., 1994).

Telomerase biogenesis and catalysis involve several steps. Formation and stabilization of the RNP complex, which includes the protein subunit TERT (telomerase reverse transcriptase) (Lingner et al., 1997) and the RNA subunit TR (telomerase RNA), occurs in the nucleus (Blackburn et al., 1989; Egan and Collins, 2012; Greider and Blackburn, 1989). The assembled telomerase RNP is then trafficked through sub-nuclear structures called Cajal bodies (Venteicher and Artandi, 2009) before it is finally recruited to telomeres for chromosome end extension (Nandakumar and Cech, 2013). Telomeres are coated by shelterin, a six-protein complex (consisting of POT1, TPP1, TIN2, TRF1, TRF2, and Rap1) that protects chromosome ends from erroneously eliciting a DNA damage response (Kibe et al., 2016; Palm and de Lange, 2008). Shelterin component TPP1 (encoded by the gene *ACD*) (Houghtaling et al., 2004; Liu et al., 2004; Ye et al., 2004) is uniquely involved in facilitating telomerase action as well. TPP1 not only binds shelterin proteins POT1 (protection of telomeres 1) and TIN2 (TERF1-interacting nuclear factor 2) (Figure 1A), but it also recruits telomerase to telomeres (Nandakumar and Cech, 2013; Palm and de Lange, 2008). The primary binding partner of TPP1 within telomerase is the TEN (telomerase essential N-terminal) domain of TERT (Schmidt et al., 2014; Sexton et al., 2012; Zaug et al., 2010; Zhong et al., 2012) (Figure S1A), although other regions of TERT including the CTE (carboxy-terminal extension or thumb) domain (Zhong et al., 2012) and the IFD (insertions in fingers domain) (Chu et al., 2016) have also been implicated in this function (Figure S1A). Once recruited, TPP1 associates with telomerase to stimulate telomerase repeat addition processivity (RAP; hereby referred to as processivity) *in vitro* and promote telomere lengthening in telomerase-positive cells (Nandakumar et al., 2012; Wang et al., 2007).

The region of TPP1 responsible for telomerase-related functions has been mapped to an OB domain (Abreu et al., 2010; Wang et al., 2007; Xin et al., 2007) (corresponding to human TPP1 amino acids [aa] 87–250 or mouse TPP1 aa 1–162; Figure 1A). In human TPP1, seven conserved and surface-exposed OB residues (E168, E169, E171, R180, L183, L212, and E215) were found to be critical for telomerase association and are collectively referred to as the TEL (TPP1 glutamate (E) and leucine (L)-rich) patch (Nandakumar et al., 2012; Sexton et al., 2012; Zhong et al., 2012) (Figure 1A; Figure S1C). The importance of the TEL patch is further highlighted by the discovery of a TPP1 K170Δ mutation in two unrelated individuals presenting with telomeropathies (Guo et al., 2014; Kocak et al., 2014). TPP1 K170Δ structurally distorts the peptide backbone of the loop harboring TEL patch glutamate residues E168, E169, and E171, resulting in telomere shortening (Bisht et al., 2016). Additionally, TPP1 knockin experiments in human

This is an open access article under the CC BY-NC-ND license (http://creativecommons.org/licenses/by-nc-nd/4.0/).

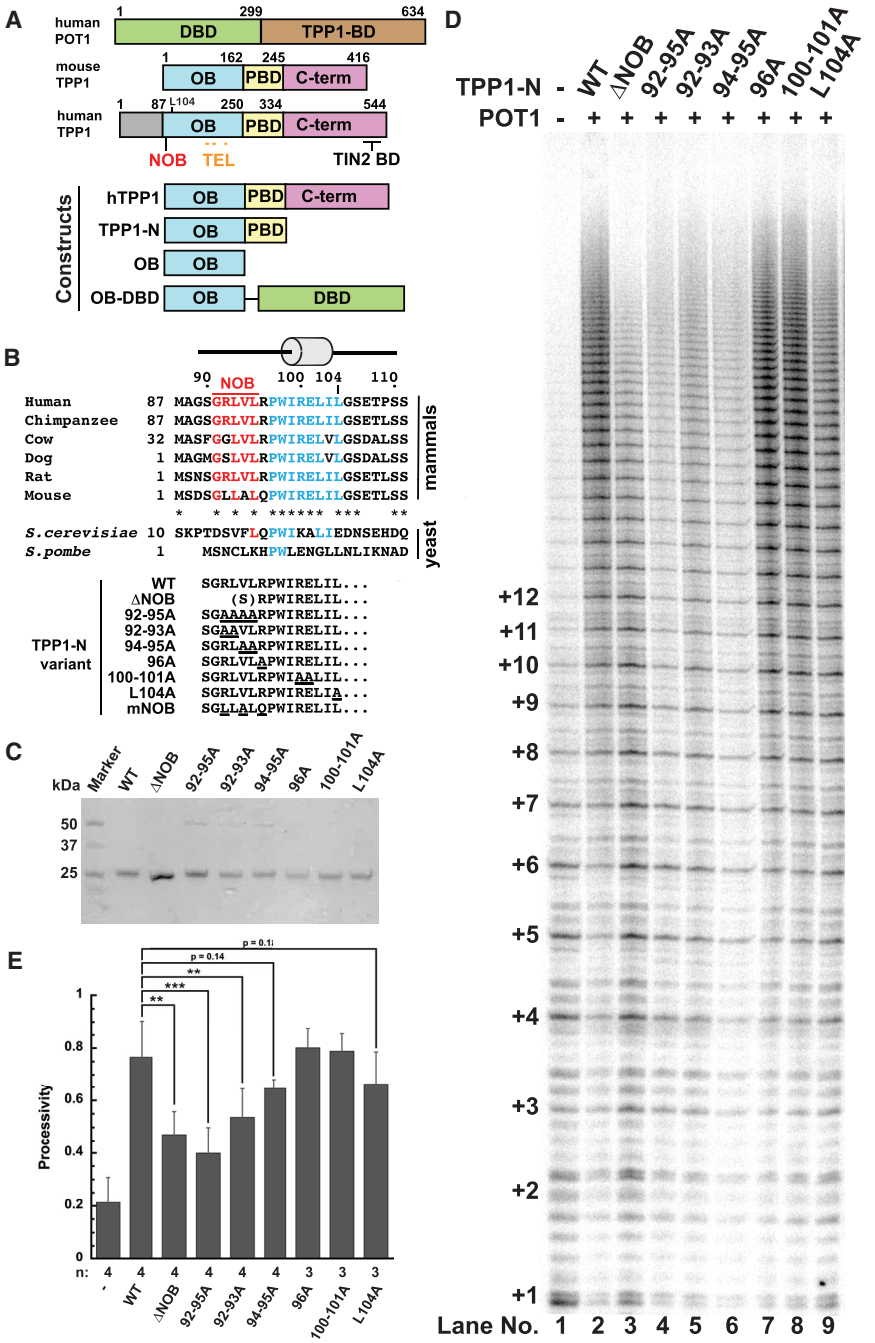

Figure 1. NOB Region of TPP1 Is Critical for Facilitating Repeat Addition Processivity of Telomerase

(A) Schematic of POT1 and TPP1 proteins and constructs used in this study. The domain organization of human POT1 (DNA-binding domain [hDBD] and TPP1-binding domain [TPP1-BD]) and mouse or human TPP1 (OB domain [OB], POT1-binding domain [PBD], and C-terminal region [C-term], which includes the TIN2-binding domain [TIN2 BD]) are shown. Amino acid numbering above the schematics indicates domain boundaries. NOB (red) and TEL patch (mustard) residues are indicated. Eighty-six aa N-terminal to Met87 in human TPP1 encode a region of unknown function somewhat conserved in primates but not other mammals.

(B) Top: Primary sequence for the N terminus of the TPP1 OB domain in representative mammals and yeast homologs Est3 (*S. cerevisiae*) and Tpz1 (*S. pombe*). Est3 protein is homologous to TPP1-OB and lacks C-terminal sequences that correspond to POT1- and TIN2-binding regions. The conserved PWI residues and first alpha helix are part of the structural core of the OB domain (shown in blue). N-terminal to this region is a largely hydrophobic sequence, the N terminus of OB domain or NOB, shown in red. Asterisks in the mammalian line-ups indicate sequence identity. Bottom: The distinctive N-termini of the TPP1-N variants analyzed in telomerase assays are shown with site-directed mutations underlined. The N terminus of the ΔNOB variant begins with a serine followed by aa R96.

(C) Coomassie-blue-stained SDS-PAGE gel of the purified TPP1-N variant proteins.

(D) Direct telomerase activity assay with purified POT1 and TPP1-N variants. Lane 1: telomerase extract alone; lanes 2–9 include POT1 and indicated TPP1-N proteins.

(E) Quantitative comparison of telomerase processivity for replicate experiments of which (D) is representative. n, number of replicates performed for each construct. Processivity is defined as the ratio of the total intensity from bands representing the addition of 9 or more hexad repeats over the total intensity in the lane (omitting repeats 1 and 2) using the rolling ball method to define background. Error bars indicate SD. **p value between 0.001 to 0.01; ***$p < 0.001$.

Statistical significance was scored with two-tailed Student's t test. See also Figures S1 and S4.

embryonic stem cells (hESCs) confirm that deletion of this acidic loop leads to severely shortened telomeres and reduced long-term cell viability (Sexton et al., 2014). Other TPP1 residues implicated in mediating telomerase function include: W98, which likely serves a structural role (Rao et al., 2014; Zhang et al., 2013); phosphorylation site S111, whose mutation altered telomere length regulation in cells (Zhang et al., 2013) through a mechanism not revealed in direct telomerase extension assays (Nandakumar et al., 2012); and L104, whose mutation reduces telomerase processivity but not association (Nandakumar et al., 2012) and which has been proposed to be involved in regulating telomere length homeostasis (Sexton et al., 2014).

The TPP1 TEL patch is necessary for telomerase regulation; however, it does not describe the entire telomerase interaction surface on TPP1. All seven TEL patch residues identified in human TPP1 are conserved in mouse TPP1 (Figure S1C), yet mouse TPP1 is unable to stimulate processivity of human telomerase (Zaug et al., 2010). N-terminal to the first alpha helix in the TPP1 OB domain resides a largely hydrophobic sequence that is well conserved among many mammals but is less

conserved between humans and mice (Figure 1B, top). In the crystal lattice formed by the human TPP1 OB domain, these residues are buried to form a homodimeric interface (Figure S1B; Wang et al., 2007). Given that the TPP1 OB domain is monomeric in solution (data not shown; Wang et al., 2007), it is likely that the hydrophobic N terminus of the OB domain (NOB) is buried in a different interface to shield it from the aqueous environment in the cell. We asked whether the NOB region of TPP1 contributes to telomerase binding and dictates human versus mouse TPP1 specificity for stimulating telomerase. Here, we show that human TPP1 NOB mutants reduce the stimulation of telomerase processivity by TPP1, abrogate telomerase recruitment to telomeres, and shorten telomeres of human cells in culture. Simply replacing mouse TPP1 NOB with the analogous residues of the human homolog improves the ability of mouse TPP1 to stimulate human telomerase. Our study reveals that the NOB region, together with the TEL patch, provides a more complete model for the surface of TPP1 that is critical for telomerase function.

RESULTS

NOB Region of TPP1 Is Critical for Stimulating Processivity of Telomerase

To determine if the N terminus of the TPP1 OB domain is important for telomerase processivity, we purified wild-type TPP1-N (TPP1 aa 90–334; TPP1-N WT) and mutant TPP1-N proteins harboring mutations or deletions within the NOB region (Figures 1A and 1B [bottom]). All TPP1 mutant and WT proteins were recombinantly expressed in *Escherichia coli* and purified as previously described (Bisht et al., 2016) (Figure 1C; see Experimental Procedures). We then performed direct telomerase primer extension assays using super-telomerase extract prepared from HEK293T cells (Cristofari and Lingner, 2006) and POT1 purified from baculovirus-infected insect cells (Figures 1D and 1E; see Experimental Procedures). TPP1-N WT displayed the characteristic increase in telomerase processivity compared with telomerase extract alone, as indicated by a larger fraction of long DNA products (Figure 1D [compare lanes 1 and 2]). Deletion of the NOB region of TPP1 (TPP1-N ΔNOB) resulted in a striking decrease in telomerase processivity compared with TPP1-N WT (38% decrease) (Figures 1D [compare lanes 2 and 3] and 1E). To pinpoint which residues within TPP1 NOB contribute to telomerase stimulation, we engineered a series of alanine mutations between TPP1 aa 92–104. Mutating residues 92–95 to alanine (92–95A) resulted in a significant decrease in telomerase processivity relative to TPP1-N WT and comparable to that of TPP1-N ΔNOB (Figures 1D [compare lanes 2–4] and 1E). TPP1-N with alanine substitutions at aa 92–93 (92–93A) or 94–95 (94–95A) similarly resulted in a decrease in processivity (Figures 1D [compare lane 2 with lanes 5 and 6] and 1E). In contrast, downstream alanine substitutions of aa 96 (96A) or aa 100–101 (100–101A) had no effect on telomerase processivity compared with WT (Figures 1D [compare lane 2 with lanes 7 and 8] and 1E). Mutation of TPP1 aa L104 has previously been shown to moderately reduce telomerase processivity (Nandakumar et al., 2012). Because L104 and the NOB region lie in close proximity, we directly compared the contributions of these regions to telomerase function. In contrast to the NOB mutants that showed a considerable decrease in telomerase processivity relative to WT, the effects of the L104A mutation were more modest (13% decrease; Figures 1D [compare lane 9 with lanes 2–5] and 1E). In summary, our data define the NOB region as a functional element within TPP1 that is critical for stimulating telomerase processivity.

Effects of the NOB Region on Telomerase Processivity Are Independent of TPP1 Binding to POT1 or TIN2

The OB domain of TPP1 has not only been implicated in telomerase binding but also in stabilizing the POT1-DNA complex (Rajavel et al., 2016). Telomerase activity and processivity measured in our primer extension assay depends not just on the TPP1-telomerase interaction but also on tethering TPP1 to POT1-bound DNA. To confirm that the defects of NOB mutants result solely from telomerase-binding deficiencies, we performed primer extension assays with a series of chimeric proteins that completely lack the POT1 and TIN2 binding regions of TPP1. In these fusions, the OB domain of human TPP1 is covalently linked to the DNA-binding domain of human POT1 (hOB-hDBD), enabling the recruitment of the TPP1 OB domain directly to the single-stranded telomeric DNA primer (Figure 1A). hOB-hDBD chimeric proteins were recombinantly expressed in *E. coli* and purified (Figure 2A; see Experimental Procedures). WT hOB-hDBD stimulated telomerase processivity to levels comparable to that of the POT1 + TPP1-N heterodimeric complex (Figures 2B [compare lanes 1–3] and 2C). To further confirm that our hOB-hDBD fusion system recapitulates the phenotypes of the covalently unlinked protein complex, we examined the E169A-E171A (EE-AA) TEL patch double mutation previously shown to be severely defective in telomerase processivity stimulation (Nandakumar et al., 2012). EE-AA in the hOB-hDBD backbone was defective in stimulating telomerase processivity (58% decrease; Figures 2B and 2C). The most instructive finding was that deletion or mutation of NOB (constructs hOB-hDBD ΔNOB and hOB-hDBD 92–95A, respectively) caused defects in telomerase processivity (43% and 61% decrease, respectively) that are comparable to that of the EE-AA mutant (Figures 2B and 2C).

To further exclude the possibility that TPP1 NOB affects TIN2 or POT1 binding, we performed co-immunoprecipitation experiments. Both transiently expressed FLAG-tagged TPP1 WT and TPP1ΔNOB bound Myc-POT1 or Myc-TIN2 on anti-FLAG conjugated beads (Figure 2D). These data confirm that the TPP1 NOB region stimulates telomerase processivity independent of POT1 or TIN2 binding.

TPP1ΔNOB Fails to Recruit Telomerase to Telomeres

Because TEL patch mutants of TPP1 fail to stimulate processivity of telomerase due to poor telomerase association (Nandakumar et al., 2012; Sexton et al., 2012; Zhong et al., 2012), we asked how deleting the NOB would affect TPP1-telomerase association in cells. To address this, we engineered stable cell lines that utilize a tetracycline-inducible promoter to control the expression of a single-copy gene cassette encoding FLAG-tagged TPP1 ΔNOB (ΔNOB; aa 96–544) or TPP1 L104A (L104A; aa 87–544) using a published method (Bisht et al., 2016; Nandakumar et al., 2012) (Figure 3A; Figure S2A). These

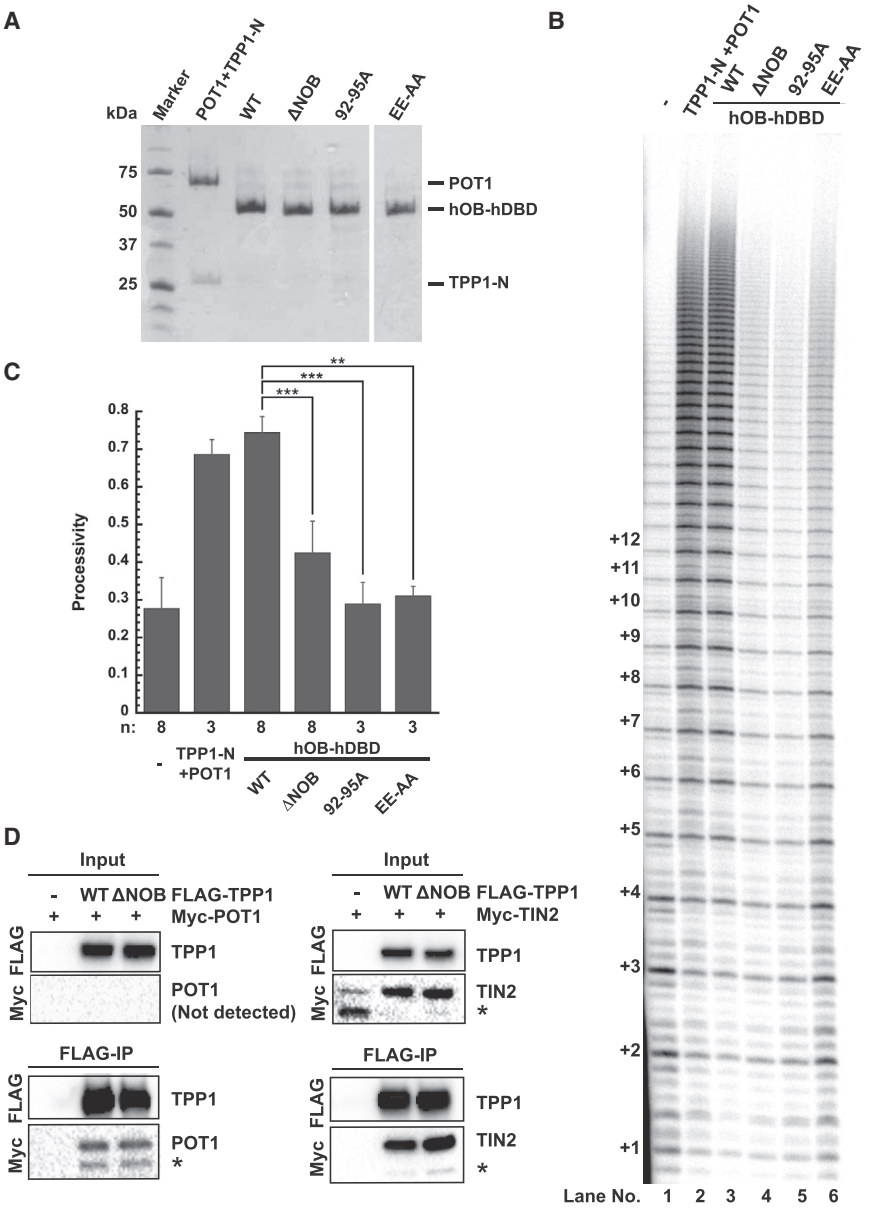

Figure 2. Effects of the NOB Region on Telomerase Processivity Are Independent of TPP1 Binding to POT1 and TIN2

(A) Coomassie-blue-stained SDS-PAGE gel of purified POT1/TPP1-N complex and hOB-hDBD fusion proteins used in (B).

(B) Direct telomerase activity assay. Lane 1: telomerase extract alone; lane 2 includes human POT1 and TPP1-N; and lanes 3–6 include the indicated hOB-hDBD variant.

(C) Quantitation of telomerase processivity from the indicated number of replicates (n), of which (B) is representative. Statistical significance was scored with a two-tailed Student's t test. Error bars indicate SD. **p value between 0.001 to 0.01; ***$p < 0.001$.

(D) Pull-down of FLAG-TPP1 (WT or ΔNOB) and Myc-POT1 or Myc-TIN2 transiently expressed in HeLa cells on anti-FLAG conjugated beads. "Input" and "FLAG-IP" immunoblots refer to soluble lysates before incubation with anti-FLAG beads and anti-FLAG beads after overnight immunoprecipitation, respectively. POT1 was not detected in the input sample but was detected in FLAG-IP samples that contained TPP1, consistent with POT1 stabilization by TPP1. Asterisks indicate POT1- and TIN2-derived degradation products.

lines were directly compared with a previously characterized TPP1 WT (WT; aa 87–544) stable cell line (Bisht et al., 2016; Nandakumar et al., 2012). Individual clones were selected to equalize FLAG-TPP1 expression levels, although we note ΔNOB consistently expressed at a higher level than WT and L104A (Figure 3A; Figure S2B). All TPP1 constructs successfully localized to telomeres (Figure S2C), in agreement with their ability to bind TIN2 and POT1. To evaluate telomerase recruitment to telomeres, we performed immunofluorescence (IF) to visualize FLAG-TPP1 and compared its localization with that of TR, which was visualized using fluorescence *in situ* hybridization (FISH). More than 90% of TPP1 WT foci co-localized with telomerase foci, indicative of robust telomerase recruitment to telomeres with TPP1 WT (Figures 3B and 3C). In contrast, cells expressing TPP1ΔNOB exhibited drastically reduced levels of telomerase recruitment (Figure 3B), with less than 20% of ΔNOB foci co-localizing with telomerase (Figure 3C; $p < 0.01$ when compared with WT). These results are consistent with what has previously been observed for TPP1 TEL patch mutations (Nandakumar et al., 2012). Although L104 is adjacent to the NOB region, previous studies suggest that L104A exhibits a small, if any, reduction in telomerase association (Nandakumar et al., 2012; Sexton et al., 2014). Indeed, L104A successfully recruited telomerase to telomeres, although a slight reduction in the percent of telomerase recruitment (relative to WT) in each L104A clone was observed ($p = 0.18$ and 0.11, respectively) (Figures 3B and 3C). The severe recruitment defects observed for the ΔNOB clones but not the L104A clones are even more striking when considering the fact that the steady-state protein levels of ΔNOB are consistently higher than that of L104A (Figure 3A; Figure S2B). In summary, despite its proximity to L104, the critical role of the NOB region in recruiting telomerase to telomeres resembles that of the TEL patch.

TPP1ΔNOB Overexpression Fails to Stimulate Telomere Lengthening in Human Cells

Although TPP1 WT overexpression induces significant telomere elongation, overexpression of TPP1 TEL patch mutants results in telomere shortening due to reduced telomerase recruitment (Nandakumar et al., 2012). Given that TPP1ΔNOB is unable to

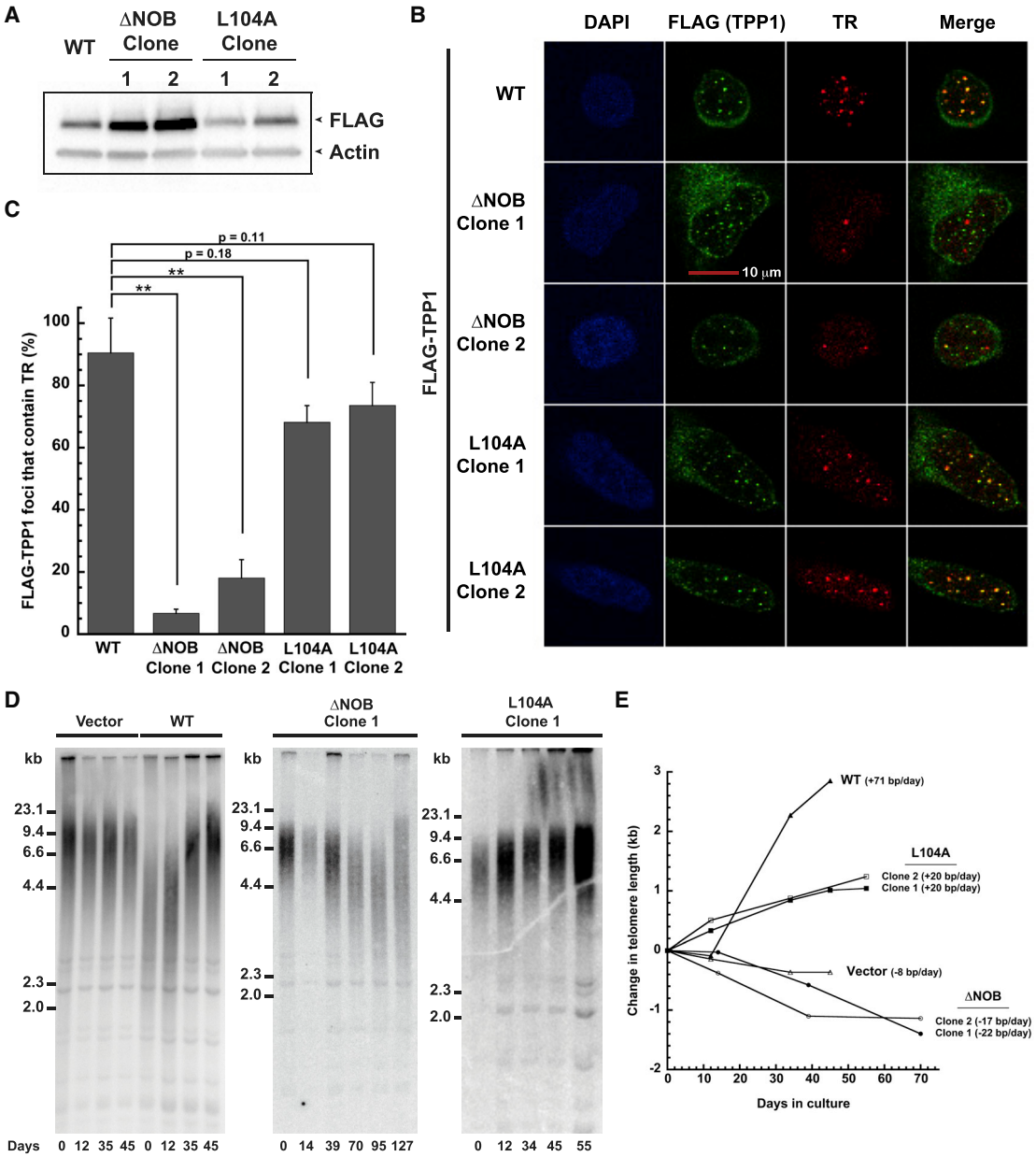

Figure 3. Deletion of the NOB of TPP1 Disrupts Both Telomerase Recruitment to Telomeres and Telomere Lengthening

(A) Immunoblot showing expression levels of FLAG-TPP1 WT or mutant protein in the indicated stable cell lines.

(B) Stable HeLa-EM2-11ht clones overexpressing the indicated FLAG-TPP1 constructs were analyzed for telomerase recruitment to telomeres using immunofluorescence-fluorescence *in situ* hybridization. "FLAG (TPP1)" shows the FLAG immunofluorescence signal indicative of telomeres (green). Fluorescence *in situ* hybridization was used to detect telomerase RNA (TR; red). "Merge": extent of recruitment of telomerase to telomeres (yellow). Scale bar, 10 μm.

(C) Quantitation of telomerase recruitment data, of which (B) is representative. The mean percentage of FLAG-TPP1 foci containing TR and SD for triplicate measurements (n = 3; >100 telomere foci scored per clone) were plotted. Statistical significance was scored with a two-tailed Student's t test. **p value between 0.001 to 0.01.

(D) Telomeric restriction fragment (TRF) Southern blot analysis of genomic DNA from HeLa-EM2-11ht cell lines stably expressing the indicated TPP1 constructs (Vector, WT, ΔNOB, and L104A) for the indicated number of days in culture.

(E) The change in mean telomere length for data shown in (D) was plotted against the number of days in culture.

See also Figure S2.

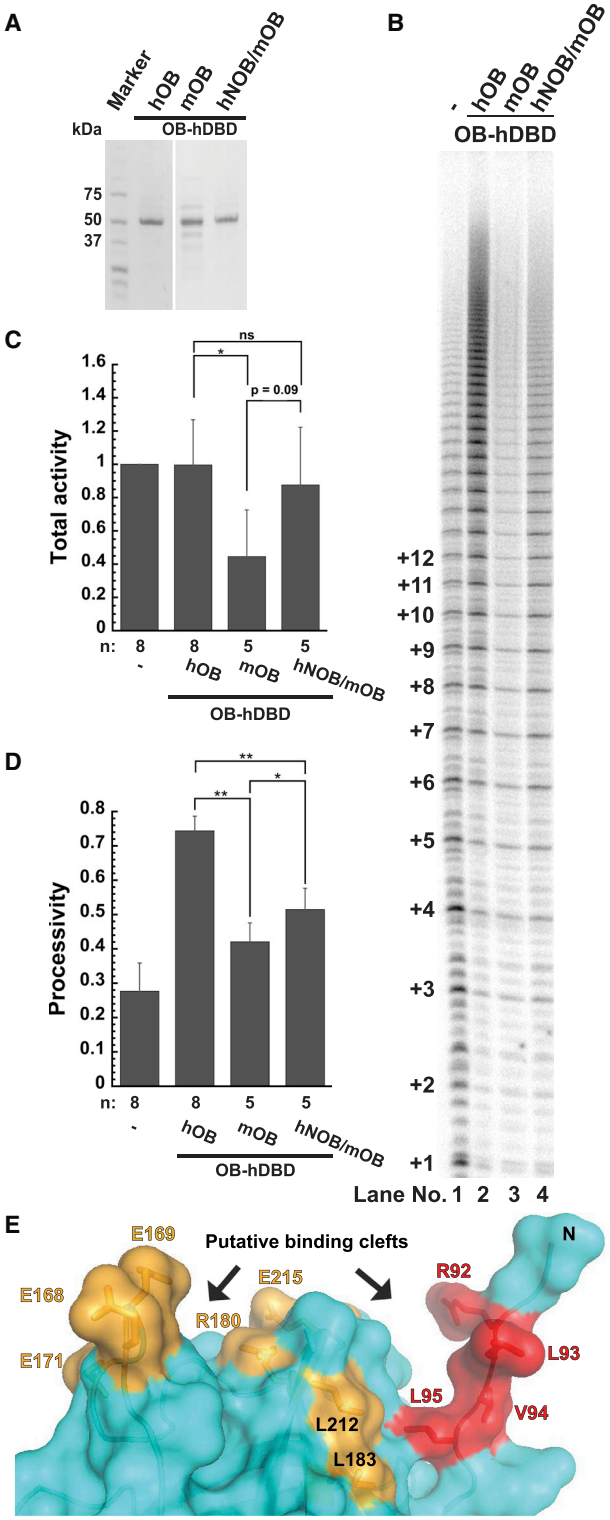

Figure 4. Inability of Mouse TPP1 to Stimulate Human Telomerase Is Partially Rescued by Including the Human NOB Sequence

(A) Coomassie-blue-stained SDS-PAGE gel of purified OB-hDBD variants containing either hTPP1 OB sequence (hOB), mTPP1 OB sequence (mOB), or mTPP1 OB sequence with site-directed mutations to reconstitute the human TPP1 NOB sequence (hNOB/mOB).

(B) Direct telomerase activity assay. Lane 1: telomerase extract alone; lanes 2–4 include indicated OB-hDBD variant.

(C and D) Quantitative comparison of (C) telomerase activity and (D) processivity from the indicated number of replicates (n), for which (B) is representative. Activity was determined using the entire signal in the lane with rolling-ball background correction, normalized against the signal observed for telomerase extract alone. Statistical significance was scored with a two-tailed Student's t test. Error bars indicate SD. *p value between 0.01 to 0.05; **p value between 0.001 to 0.01.

(E) The NOB (red) and TEL patch (mustard) residues in the structure of the human TPP1 OB domain (PDB: 2I46; Wang et al., 2007) line two prominent clefts (indicated with arrows) that could bind telomerase.

See also Figures S3 and S4.

efficiently recruit telomerase to telomeres, we asked how deleting the TPP1 NOB region would affect telomere length maintenance. For this, we conducted telomere restriction fragment (TRF) length analysis of our engineered stable cell lines overexpressing TPP1 WT, ΔNOB, and L104A proteins. A stable cell line containing the tetracycline-inducible promoter but an empty cassette (vector) was engineered and propagated in parallel to serve as a negative control. As expected, the telomeres of the vector cell line remained relatively stable over 45 days in culture, similar to those of untransfected HeLa cells (Nandakumar et al., 2012) (Figures 3D and 3E). Overexpression of TPP1 WT led to a robust increase in telomere length over time (~70 bp/day) (Figures 3D and 3E), consistent with previous reports (Bisht et al., 2016; Nakashima et al., 2013; Nandakumar et al., 2012). In sharp contrast, overexpression of TPP1ΔNOB resulted in a decrease in telomere length (Figure 3D; Figure S2D) at a rate of 22 and 17 bp per day for clones 1 and 2, respectively (Figure 3E). This rate of telomere shortening is reminiscent of that observed for the TPP1 EE-AA TEL-patch-mutant-expressing cells (~18 bp/day) (Bisht et al., 2016; Nakashima et al., 2013; Nandakumar et al., 2012). The eventual rescue of telomere length observed in prolonged cultures of TPP1ΔNOB stable cell lines (Figure 3D; Figure S2D) coincided with a loss of TPP1ΔNOB expression (Figure S2E), an effect previously documented for cell lines expressing TEL patch mutants (Nakashima et al., 2013). In contrast to this trend, L104A overexpression resulted in a constant increase in telomere length (Figure 3D; Figure S2D) at a rate of 20 bp per day for each clone. The rate of telomere elongation for L104A (Figure 3E) was less dramatic than that of WT, which is in accordance with our biochemical (Figures 1D and 1E) and cytological data (Figures 3B and 3C). From these data, we conclude that the critical role of TPP1 NOB in telomere length maintenance closely resembles that of the previously identified TEL patch.

The Human TPP1 NOB Region Improves Stimulation of Human Telomerase by Mouse TPP1

Given that some NOB residues are different between mouse and human TPP1 (Figure 1B; top), we asked whether the mouse NOB sequence (mNOB) accounts for the inability of mouse TPP1 to stimulate human telomerase (Zaug et al., 2010). To address this, we exploited our OB-hDBD fusion system so that species-specific differences in POT1-TPP1 binding would not influence our results. We purified a chimera in which the mouse TPP1 OB domain was engineered upstream of hDBD (mOB-hDBD) (Figure 4A; Figure S3A). The chimeric mOB-hDBD protein

successfully stimulated telomerase reconstituted with mouse TERT protein (mTERT) (Figure S3B [compare lanes 8–10 with 4–6]). In sharp contrast, mOB-hDBD was defective in stimulating human telomerase activity or processivity compared with hOB-hDBD (Figures 4B [compare lanes 1–3], 4C, and 4D; for replicate, compare lanes 3 and 7 in Figure S3B). We next asked whether replacing the human NOB sequence (hNOB) with mNOB in human TPP1 (Figure 1B; bottom) would compromise human telomerase processivity. Indeed, hTPP1-N mNOB reduced human telomerase processivity relative to hTPP1-N WT (Figure S3B [compare lanes 1 and 2]). Finally, to test whether human NOB can revive mOB-hDBD function with human telomerase, we designed a variant in which three of the mouse NOB residues (L6R, A8V, and Q10R) were replaced with their human equivalents in mOB-hDBD (hNOB/mOB-hDBD) (Figure 4A; Figure S3A; see Experimental Procedures). Compared with mOB-hDBD, the chimeric hNOB/mOB-hDBD protein was able to partially stimulate both processivity and activity of human telomerase (Figures 4B [compare lanes 3 and 4], 4C, and 4D). We conclude that the NOB region is an important determinant of mouse versus human species-specificity of the TPP1-telomerase interaction. However, hNOB/mOB-hDBD did not completely rescue the activity and processivity of telomerase to the levels observed with WT hOB-hDBD (Figures 4B [compare lanes 2 and 4], 4C, and 4D), indicating that the complete telomerase-binding surface of TPP1 exceeds the list of identified TEL patch and NOB residues.

DISCUSSION

TPP1 is the telomere-associated factor that is primarily responsible for recruiting telomerase to chromosome ends. Mutagenesis screens by three independent groups converged on a strictly conserved surface of TPP1 OB, called the TEL patch, as being a critical determinant of telomerase action (Nandakumar et al., 2012; Sexton et al., 2012; Zhong et al., 2012). In this study, we uncover NOB as another distinct element in TPP1 that is critical for telomerase function, but which likely escaped discovery because it is less conserved between mice and humans. We show that deletion or mutation of human TPP1 NOB residues results in a reduced ability to stimulate telomerase processivity, diminished telomerase recruitment, and shortening of telomeres in cells. Furthermore, the extreme phenotype of deleting the NOB region matches that of mutations within the TEL patch, suggesting that both of these TPP1 elements are critical for telomerase function.

Inspection of the crystal structure of TPP1 OB reveals that, although distant from the acidic residues of the TEL patch (E168, E169, and E171), the hydrophobic NOB region is proximal to TEL patch residues L183 and L212 (Figure 4E). Labeling both TEL patch and NOB residues on the surface of TPP1, two clefts for binding telomerase emerge, one laced with primarily acidic residues (E168, E169, E171, R180, and E215), and another with largely hydrophobic residues (R92, L93, V94, L95, L183, and L212) (Figure 4E). Analysis of TERT has revealed the highly basic TEN domain as the binding partner of the TEL patch (Sexton et al., 2012; Zhong et al., 2012) (Figure S1A). However, only one binary interaction between TPP1 and telomerase (TERT K78 and TPP1 E215) has been firmly established (Schmidt et al., 2014) (Figure S1A). The IFD of TERT has also been suggested as a potential binding partner of TPP1 based on observations that TERT IFD mutant V791Y is neither recruited efficiently to telomeres nor stimulated by TPP1 in primer extension analysis (Chu et al., 2016) (Figure S1A). Finally, the CTE domain of TERT has also been proposed to contact TPP1 (Zhong et al., 2012) (Figure S1A). Based on the presence of two distinct telomerase-binding clefts in TPP1 OB, it is tempting to speculate that the highly basic TEN domain docks into the acidic cleft, while the hydrophobic pocket is occupied by residues residing elsewhere in TERT.

Given the importance of the TPP1 NOB region in stimulating telomerase processivity, it is intriguing that the N-terminal regions of the distant yet well-characterized TPP1 homologs Tpz1 of the fission yeast *S. pombe* (Miyoshi et al., 2008), TEBPβ of ciliate *S. nova*, and Est3 of budding yeast *S. cerevisiae* all show structural similarities to mammalian TPP1 (Horvath et al., 1998; Rao et al., 2014; Wang et al., 2007). In each, the N terminus contains an integral alpha helix that precedes the canonical beta barrel core (prediction, in the case of Tpz1). In both mammals and budding yeast, the NOB region borders this helix, which is capped at its N terminus by a "PWI" sequence (Figure 1B; top). In the structures of Est3 and human TPP1, the conserved tryptophan is stabilized by an essential aspartate located in a loop between the second and third beta strands of the OB domain (Lubin et al., 2013; Rao et al., 2014) that has also been identified as important for DNA binding with POT1 (Rajavel et al., 2016). Both the tryptophan and the aspartate residues are conserved in Tpz1, and an analogous interaction occurs in ciliate TEBPβ with a phenylalanine taking the place of the tryptophan (Rao et al., 2014). Given that the structural elements at the N terminus of the OB domain of distant TPP1 homologs are so well conserved, it is possible that the NOB region similarly facilitates telomerase recruitment in at least some of these diverse eukaryotic organisms.

In human TPP1, the first alpha helix of the N-terminal OB domain terminates at L104 (Wang et al., 2007). Mutation of L104 does not influence telomerase binding to TPP1 (Nandakumar et al., 2012), but when introduced at the endogenous gene locus in hESCs, it causes resetting of telomere length to a lower length without affecting long-term viability (Sexton et al., 2014). Yet only subtle telomerase recruitment and telomere length phenotypes of L104A were observed in the overexpression system used in the current study. These results open the possibility that L104 allosterically affects telomerase function through the NOB region that resides at the opposite end (i.e., N terminus) of the helix harboring L104. Alternatively, phenotypes of L104 mutants may result from protein folding/stability defects in TPP1, as the low B-factor of L104 in the crystal structure suggests a structural role for this residue. This possibility is consistent with the fact that in multiple clones, we observed that steady-state levels of L104A were lower than that of both WT and ΔNOB (Figure S2B).

Sequence conservation is a powerful tool to probe protein structure and function, including protein-protein interactions. It was through mutagenesis of strictly conserved surface residues that the TEL patch of TPP1 was mapped (Figure S1C). However,

telomere-telomerase interaction is species specific (Zaug et al., 2010), which suggests there are key determinants of the TPP1-telomerase-binding surface that are not strictly conserved. In fact, the NOB region embodies one such species-specific element in TPP1 that is important for telomerase function. However, hNOB/mOB-hDBD, despite harboring all seven TEL patch residues and the human TPP1 NOB sequence, is not able to stimulate telomerase processivity to hOB-hDBD levels (Figures 4B–4D). Further mutagenesis exploiting differences in mouse versus human TPP1 sequences will provide an efficient avenue to completely define the telomerase-binding surface of TPP1. The sheer size combined with the macromolecular complexity of the telomerase RNP has been a major impediment to comprehensively determining the TPP1-binding surface of telomerase. We propose that probing species-specific sequence differences and involving cross-species hybrid proteins of TERT will greatly streamline the search for the more elusive half of the TPP1-telomerase interface.

EXPERIMENTAL PROCEDURES

Primer Extension Assay

Extension assays included super telomerase extract, 1 μM primer 5′-TTAG GGTTAGCGTTAGGG-3′, deoxynucleotide triphosphates (dNTPs), α^{32}P-deoxyguanosine triphosphate (dGTP), and 500 nM of POT1/TPP1-N variant or OB-hDBD chimeras and were performed for 1 hr at ~30°C. Extension products were resolved on a 10% polyacrylamide/7 M urea/1× Tris-borate-EDTA (TBE) sequencing gel, and the data were imaged using a Phosphorimager (Storm; GE Healthcare Life Sciences). Activity was scored by quantitating the signal for the entire lane. Processivity values were obtained by dividing the total intensity from bands representing the addition of 9 or more hexad repeats by the total intensity in the lane (omitting repeats 1 and 2) using the rolling ball method to define background.

IF and FISH Microscopy

Cells were fixed with 4% formaldehyde in PBS for 10 min and permeabilized in PBS containing 0.5% Triton X-100 for 10 min. IF was first performed to visualize FLAG-TPP1 proteins using mouse monoclonal anti-FLAG M2 (Sigma; F1804; 1:500) in combination with Alexa-Fluor-568-conjugated anti-mouse immunoglobulin G (IgG; Life Technologies). Cy5-conjugated probes complementary to TR were used to detect TR by FISH. The cells were mounted on microscope slides using ProLong Gold mounting medium with 4',6-diamidino-2-phenylindole (DAPI) (Life Technologies). A laser scanning confocal microscope (SP5; Leica, Germany) was used for imaging, and images obtained were processed with ImageJ and Adobe Photoshop. Co-localizations were quantified manually by two separate individuals.

TRF Length Analysis

Genomic DNA purified by the GenElute Kit (Sigma, G1N350-1KT) was digested with *HinfI* and *RsaI*. The digested DNA was resolved on a 0.8% agarose-1× TBE gel, which was then imaged with a fluorescent ruler and dried at 55°C for 1 hr before denaturation in 0.5 M NaOH. After neutralization with 1.5 M NaCl and 0.5 M Tris-Cl (pH 7.5), the gel was prehybridized in Church buffer at 65°C and probed with 5′ ^{32}P-labeled $(TTAGGG)_4$ oligonucleotide overnight at 55°C. After washing with 2× saline sodium citrate (SSC) at 55°C, the gel was imaged using phosphorimaging, analyzed using Imagequant TL software, and calibrated using the molecular weights of the lambda DNA-HindIII digest ladder. The mean telomere length for each lane was plotted as a function of days in culture.

Statistical Analysis

Data are expressed as mean ± SD. The statistical significance of differences between groups was examined using two-tailed Student's t test.

See Supplemental Experimental Procedures for further details.

SUPPLEMENTAL INFORMATION

Supplemental Information includes Supplemental Experimental Procedures and four figures and can be found with this article online at https://doi.org/10.1016/j.celrep.2018.01.012.

ACKNOWLEDGMENTS

We thank Devon Pendlebury and Eric Smith for critical feedback; Dr. Laura Buttitta for Alexa Fluor 633 anti-mouse IgG; Dr. Gregg Sobocinski for help with microscopy; and Dr. Lindsay Matthews for help with Gibson Assembly. This work was funded by NIH grants R00CA167644 (to J.N.), R01GM120094 (to J.N.), R01AG050509 (to J.N.; co-investigator), and T32GM007544 (to the University of Michigan Genetics Training Program; S.G. was a trainee) and by American Cancer Society Research Scholar grant RSG-17-037-01-DMC (to J.N.).

AUTHOR CONTRIBUTIONS

V.M.T. conceived the idea of mutating TPP1 NOB. All authors contributed to experimental design and cloning. V.M.T. performed protein and telomerase extract preparations and telomerase activity assays. S.G. performed stable cell line generation, co-immunoprecipitation, IF-FISH, and TRF analysis. All authors contributed to data analysis. S.G. wrote the manuscript with detailed input from V.M.T. and J.N.

DECLARATION OF INTERESTS

The authors declare no competing interests.

Received: October 20, 2017
Revised: December 19, 2017
Accepted: January 3, 2018
Published: January 30, 2018

REFERENCES

Abreu, E., Aritonovska, E., Reichenbach, P., Cristofari, G., Culp, B., Terns, R.M., Lingner, J., and Terns, M.P. (2010). TIN2-tethered TPP1 recruits human telomerase to telomeres in vivo. Mol. Cell. Biol. *30*, 2971–2982.

Bisht, K., Smith, E.M., Tesmer, V.M., and Nandakumar, J. (2016). Structural and functional consequences of a disease mutation in the telomere protein TPP1. Proc. Natl. Acad. Sci. USA *113*, 13021–13026.

Blackburn, E.H., Greider, C.W., Henderson, E., Lee, M.S., Shampay, J., and Shippen-Lentz, D. (1989). Recognition and elongation of telomeres by telomerase. Genome *31*, 553–560.

Chu, T.W., D'Souza, Y., and Autexier, C. (2016). The insertion in fingers domain in human telomerase can mediate enzyme processivity and telomerase recruitment to telomeres in a TPP1-dependent manner. Mol. Cell. Biol. *36*, 210–222.

Cristofari, G., and Lingner, J. (2006). Telomere length homeostasis requires that telomerase levels are limiting. EMBO J. *25*, 565–574.

Dokal, I. (2011). Dyskeratosis congenita. Hematology (Am. Soc. Hematol. Educ. Program) *2011*, 480–486.

Egan, E.D., and Collins, K. (2012). Biogenesis of telomerase ribonucleoproteins. RNA *18*, 1747–1759.

Greider, C.W., and Blackburn, E.H. (1985). Identification of a specific telomere terminal transferase activity in Tetrahymena extracts. Cell *43*, 405–413.

Greider, C.W., and Blackburn, E.H. (1989). A telomeric sequence in the RNA of Tetrahymena telomerase required for telomere repeat synthesis. Nature *337*, 331–337.

Guo, Y., Kartawinata, M., Li, J., Pickett, H.A., Teo, J., Kilo, T., Barbaro, P.M., Keating, B., Chen, Y., Tian, L., et al. (2014). Inherited bone marrow failure associated with germline mutation of ACD, the gene encoding telomere protein TPP1. Blood *124*, 2767–2774.

Hahn, W.C., Counter, C.M., Lundberg, A.S., Beijersbergen, R.L., Brooks, M.W., and Weinberg, R.A. (1999). Creation of human tumour cells with defined genetic elements. Nature *400*, 464–468.

Horvath, M.P., Schweiker, V.L., Bevilacqua, J.M., Ruggles, J.A., and Schultz, S.C. (1998). Crystal structure of the Oxytricha nova telomere end binding protein complexed with single strand DNA. Cell *95*, 963–974.

Houghtaling, B.R., Cuttonaro, L., Chang, W., and Smith, S. (2004). A dynamic molecular link between the telomere length regulator TRF1 and the chromosome end protector TRF2. Curr. Biol. *14*, 1621–1631.

Kibe, T., Zimmermann, M., and de Lange, T. (2016). TPP1 blocks an ATR-mediated resection mechanism at telomeres. Mol. Cell *61*, 236–246.

Kim, N.W., Piatyszek, M.A., Prowse, K.R., Harley, C.B., West, M.D., Ho, P.L., Coviello, G.M., Wright, W.E., Weinrich, S.L., and Shay, J.W. (1994). Specific association of human telomerase activity with immortal cells and cancer. Science *266*, 2011–2015.

Kocak, H., Ballew, B.J., Bisht, K., Eggebeen, R., Hicks, B.D., Suman, S., O'Neil, A., Giri, N., Maillard, I., Alter, B.P., et al.; NCI DCEG Cancer Genomics Research Laboratory; NCI DCEG Cancer Sequencing Working Group (2014). Hoyeraal-Hreidarsson syndrome caused by a germline mutation in the TEL patch of the telomere protein TPP1. Genes Dev. *28*, 2090–2102.

Lingner, J., Hughes, T.R., Shevchenko, A., Mann, M., Lundblad, V., and Cech, T.R. (1997). Reverse transcriptase motifs in the catalytic subunit of telomerase. Science *276*, 561–567.

Liu, D., Safari, A., O'Connor, M.S., Chan, D.W., Laegeler, A., Qin, J., and Songyang, Z. (2004). PTOP interacts with POT1 and regulates its localization to telomeres. Nat. Cell Biol. *6*, 673–680.

Lubin, J.W., Rao, T., Mandell, E.K., Wuttke, D.S., and Lundblad, V. (2013). Dissecting protein function: an efficient protocol for identifying separation-of-function mutations that encode structurally stable proteins. Genetics *193*, 715–725.

Miyoshi, T., Kanoh, J., Saito, M., and Ishikawa, F. (2008). Fission yeast Pot1-Tpp1 protects telomeres and regulates telomere length. Science *320*, 1341–1344.

Nakashima, M., Nandakumar, J., Sullivan, K.D., Espinosa, J.M., and Cech, T.R. (2013). Inhibition of telomerase recruitment and cancer cell death. J. Biol. Chem. *288*, 33171–33180.

Nandakumar, J., and Cech, T.R. (2013). Finding the end: recruitment of telomerase to telomeres. Nat. Rev. Mol. Cell Biol. *14*, 69–82.

Nandakumar, J., Bell, C.F., Weidenfeld, I., Zaug, A.J., Leinwand, L.A., and Cech, T.R. (2012). The TEL patch of telomere protein TPP1 mediates telomerase recruitment and processivity. Nature *492*, 285–289.

Palm, W., and de Lange, T. (2008). How shelterin protects mammalian telomeres. Annu. Rev. Genet. *42*, 301–334.

Rajavel, M., Orban, T., Xu, M., Hernandez-Sanchez, W., de la Fuente, M., Palczewski, K., and Taylor, D.J. (2016). Dynamic peptides of human TPP1 fulfill diverse functions in telomere maintenance. Nucleic Acids Res. *44*, 10467–10479.

Rao, T., Lubin, J.W., Armstrong, G.S., Tucey, T.M., Lundblad, V., and Wuttke, D.S. (2014). Structure of Est3 reveals a bimodal surface with differential roles in telomere replication. Proc. Natl. Acad. Sci. USA *111*, 214–218.

Savage, S.A. (2014). Human telomeres and telomere biology disorders. Prog. Mol. Biol. Transl. Sci. *125*, 41–66.

Schmidt, J.C., Dalby, A.B., and Cech, T.R. (2014). Identification of human TERT elements necessary for telomerase recruitment to telomeres. eLife *3*, e03563.

Sexton, A.N., Youmans, D.T., and Collins, K. (2012). Specificity requirements for human telomere protein interaction with telomerase holoenzyme. J. Biol. Chem. *287*, 34455–34464.

Sexton, A.N., Regalado, S.G., Lai, C.S., Cost, G.J., O'Neil, C.M., Urnov, F.D., Gregory, P.D., Jaenisch, R., Collins, K., and Hockemeyer, D. (2014). Genetic and molecular identification of three human TPP1 functions in telomerase action: recruitment, activation, and homeostasis set point regulation. Genes Dev. *28*, 1885–1899.

Shay, J.W., and Wright, W.E. (2010). Telomeres and telomerase in normal and cancer stem cells. FEBS Lett. *584*, 3819–3825.

Venteicher, A.S., and Artandi, S.E. (2009). TCAB1: driving telomerase to Cajal bodies. Cell Cycle *8*, 1329–1331.

Wang, F., Podell, E.R., Zaug, A.J., Yang, Y., Baciu, P., Cech, T.R., and Lei, M. (2007). The POT1-TPP1 telomere complex is a telomerase processivity factor. Nature *445*, 506–510.

Xin, H., Liu, D., Wan, M., Safari, A., Kim, H., Sun, W., O'Connor, M.S., and Songyang, Z. (2007). TPP1 is a homologue of ciliate TEBP-beta and interacts with POT1 to recruit telomerase. Nature *445*, 559–562.

Ye, J.Z., Hockemeyer, D., Krutchinsky, A.N., Loayza, D., Hooper, S.M., Chait, B.T., and de Lange, T. (2004). POT1-interacting protein PIP1: a telomere length regulator that recruits POT1 to the TIN2/TRF1 complex. Genes Dev. *18*, 1649–1654.

Zaug, A.J., Podell, E.R., Nandakumar, J., and Cech, T.R. (2010). Functional interaction between telomere protein TPP1 and telomerase. Genes Dev. *24*, 613–622.

Zhang, Y., Chen, L.Y., Han, X., Xie, W., Kim, H., Yang, D., Liu, D., and Songyang, Z. (2013). Phosphorylation of TPP1 regulates cell cycle-dependent telomerase recruitment. Proc. Natl. Acad. Sci. USA *110*, 5457–5462.

Zhong, F.L., Batista, L.F., Freund, A., Pech, M.F., Venteicher, A.S., and Artandi, S.E. (2012). TPP1 OB-fold domain controls telomere maintenance by recruiting telomerase to chromosome ends. Cell *150*, 481–494.

Cell Reports, Volume *22*

Supplemental Information

The N Terminus of the OB Domain of Telomere Protein TPP1 Is Critical for Telomerase Action

Sherilyn Grill, Valerie M. Tesmer, and Jayakrishnan Nandakumar

Figure S1

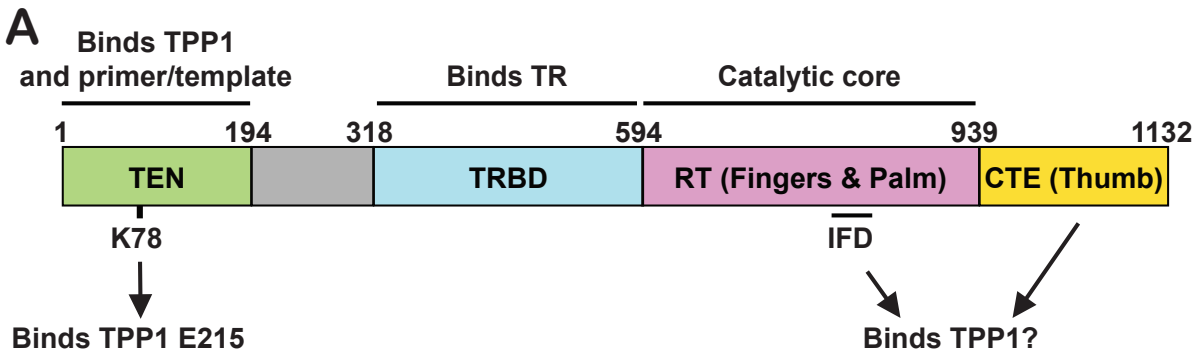

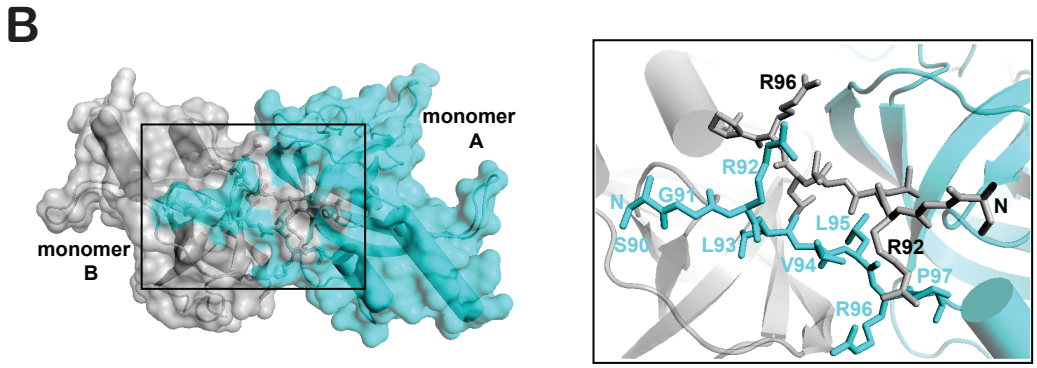

C

```
                160        170        180        190   210        220
Human           EALDTSDWEEKEFGFRGTEGRLLLLQDCGVH....SLLPTEQPRLR
Chimpanzee      EALDTSDWEEKEFGFRGTEGRLLLLQDCGVH....SLLPTEQPRLR
Cow             EALNASDWEEKEFGFRGTEGRILLLRDCKVS....ALLPTEQPREQ
Dog             EALNASDWEEKEFGFRGAEGRLLLLQDCGVR....SLLPTEQPLER
Rat             NAIDTSDWEEKEFGFRGTEGRLLLLQACGLR....NLLPTEQPRVQ
Mouse           NAIDTSDWEEKELGFRGTEGRLLLLQACGLR....NLLPTEQPRIQ
                :*:::*******:****:***:***. * :       *******  .
```

Figure S1. Structure of TPP1 OB, and domain diagram and binding properties of human TERT, Related to Figure 1. (A) The arrangement of the TEN, TRBD (telomerase RNA binding domain), RT (reverse transcriptase), and CTE (C-terminal extension) domains in the primary structure of human TERT is shown along with annotations for various (known and putative) binding regions (Gillis et al., 2008; Wang and Feigon, 2017). (B) The TPP1 N-terminal residues 90-96 (NH_2-SGRLVLR-COOH), which include the NOB region, of two OB monomers (labeled A and B) form extended conformations and align roughly anti-parallel to each other to mediate homodimerization in the human TPP1 OB domain crystal structure (PDB accession: 2I46) (Wang et al., 2007). The overall structure is shown as a surface model and the site of dimerization (boxed area) is also shown on the right in stick representation for aa 90-96. (C) The TEL patch is highly conserved across mammalian species. Sequence alignment of selected

regions of indicated TPP1 homologs with TEL patch residues shown in orange. Amino acid numbers represent the human sequence. “ * ” beneath sequence lineups indicate identical residues, “ : ” represent strongly conserved residues, and “ . ” represent weakly conserved residues as described by the MUSCLE algorithm.

Figure S2

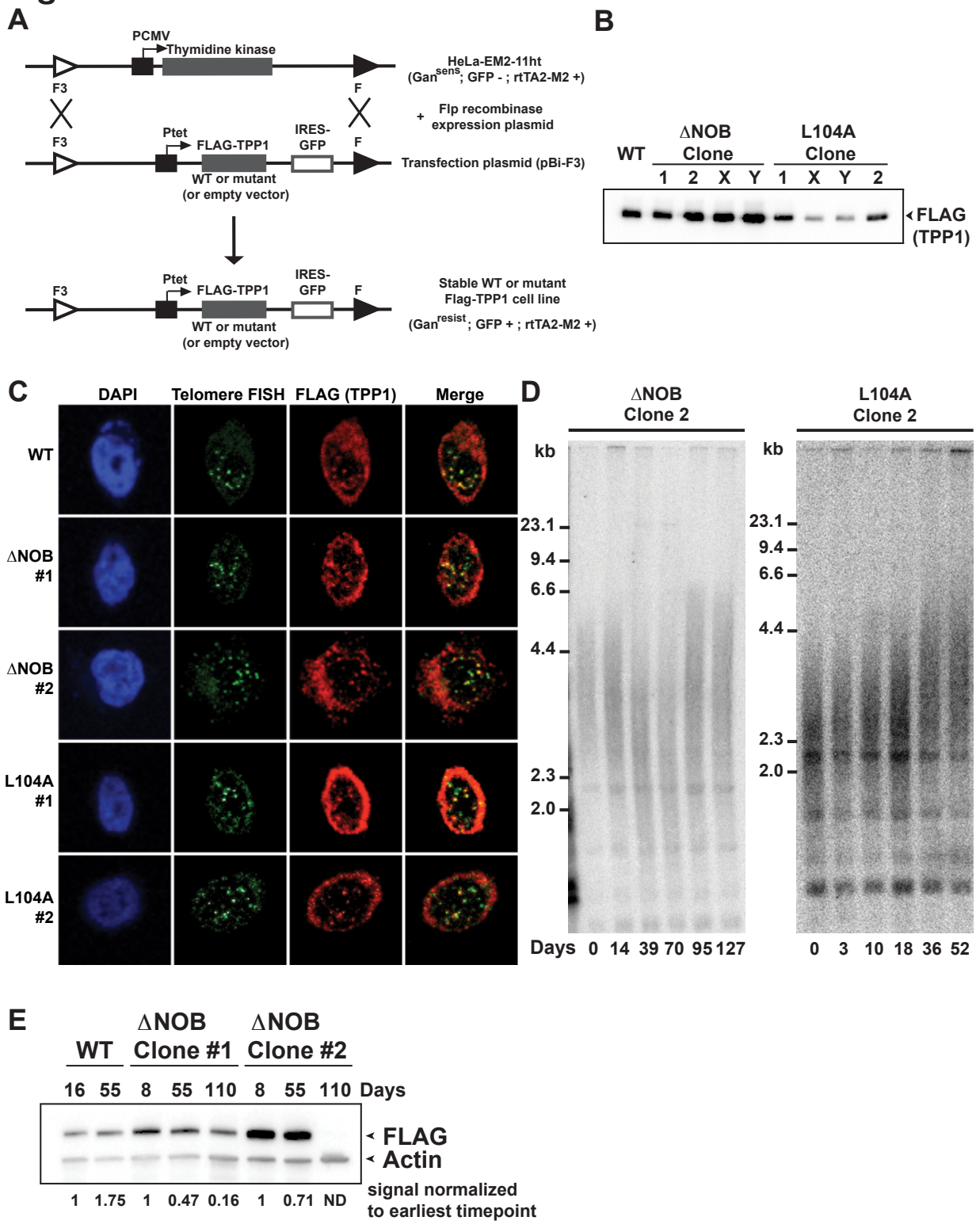

Figure S2. Cell lines stably expressing TPP1 variants for telomere lengthening and telomerase recruitment studies, Related to Figure 3. (A) Scheme for generating cell lines stably integrated with TPP1 WT or mutant, or empty

vector sequence. (B) Western blot for four clones each of ΔNOB and L104A alongside a WT clone shows high expression for ΔNOB and low expression for L104A. Clones 1 and 2 of each mutant were selected for further analysis of telomerase recruitment and telomere length. (C) IF-FISH to show colocalization of indicated TPP1 constructs with telomeres. "FLAG (TPP1)" shows the FLAG immunofluorescence signal indicative of TPP1 (red), and "Telomere FISH" indicates telomeric DNA probed with a C-rich, Cy3-labeled PNA probe (green). Merge panels reveal colocalization of TPP1 variants with telomeric DNA (yellow). (D) Telomeric restriction fragment (TRF) analysis of clone 2 for HeLa-EM2-11ht cell lines stably expressing the indicated TPP1 constructs (ΔNOB and L104A) for the indicated number of days in culture. (E) FLAG immunoblots from indicated cell lines at indicated days in culture. The FLAG signal was divided by the actin signal in each lane to account for loading differences. The numbers below the blot indicate actin-normalized FLAG signal in that lane divided by the corresponding signal in the earliest time-point for that clone.

Figure S3

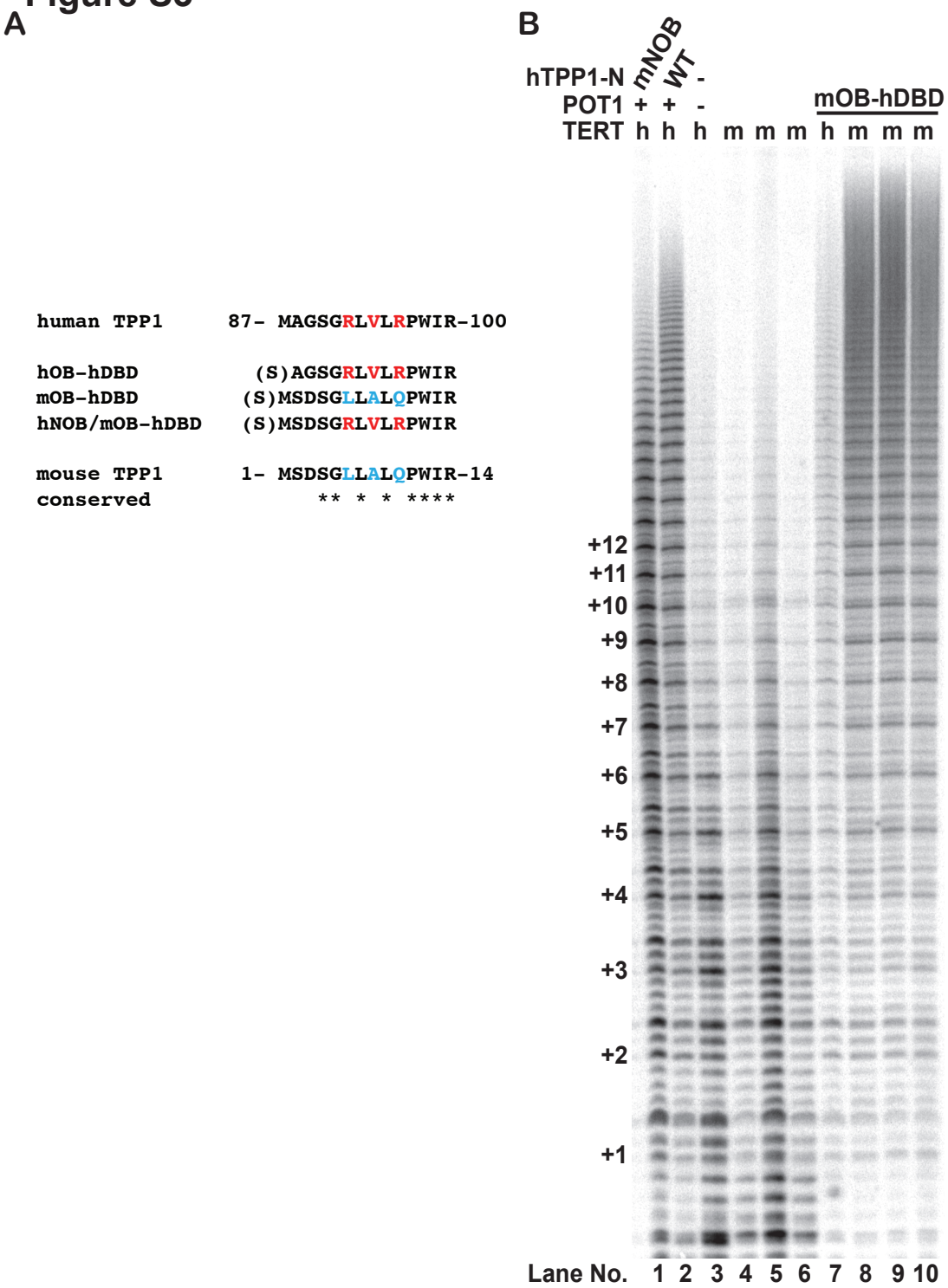

Figure S3. Mouse-human hybrid OB-DBD constructs, Related to Figure 4. (A) Schematic of N-termini for mouse and human OB-DBD variants compared with wild-type sequence for human TPP1 (above) and mouse TPP1 (below). Conserved amino acids between these N-termini are marked with asterisks. (B) Mouse NOB stimulates

reconstituted mouse telomerase but not human telomerase. Direct activity assay using extracts with telomerase reconstituted in HEK 293T cells from hTR and either hTERT (human telomerase) or mTERT (mouse telomerase). Lane 1: human telomerase plus human POT1 and TPP1-N mNOB; lane 2: human telomerase plus human POT1/ TPP1-N WT; lane 3: human telomerase extract alone; lanes 4-6: mouse telomerase reconstituted with differing ratios of transfected mTERT/TR plasmids (mTERT/TR is 1:3 in lane 4, 1:1 in lane 5, and 3:1 in lane 6); lane 7: human telomerase (hTERT/TR = 1:3) plus mOB-hDBD; lanes 8-10: same as lanes 4-6 except that mOB-hDBD was included in the reaction. hTR was used to reconstitute activity with mTERT, because telomerase reconstituted with mTR exhibits very low telomerase processivity, as previously described (Chen and Greider, 2003; Zaug et al., 2010).

Figure S4

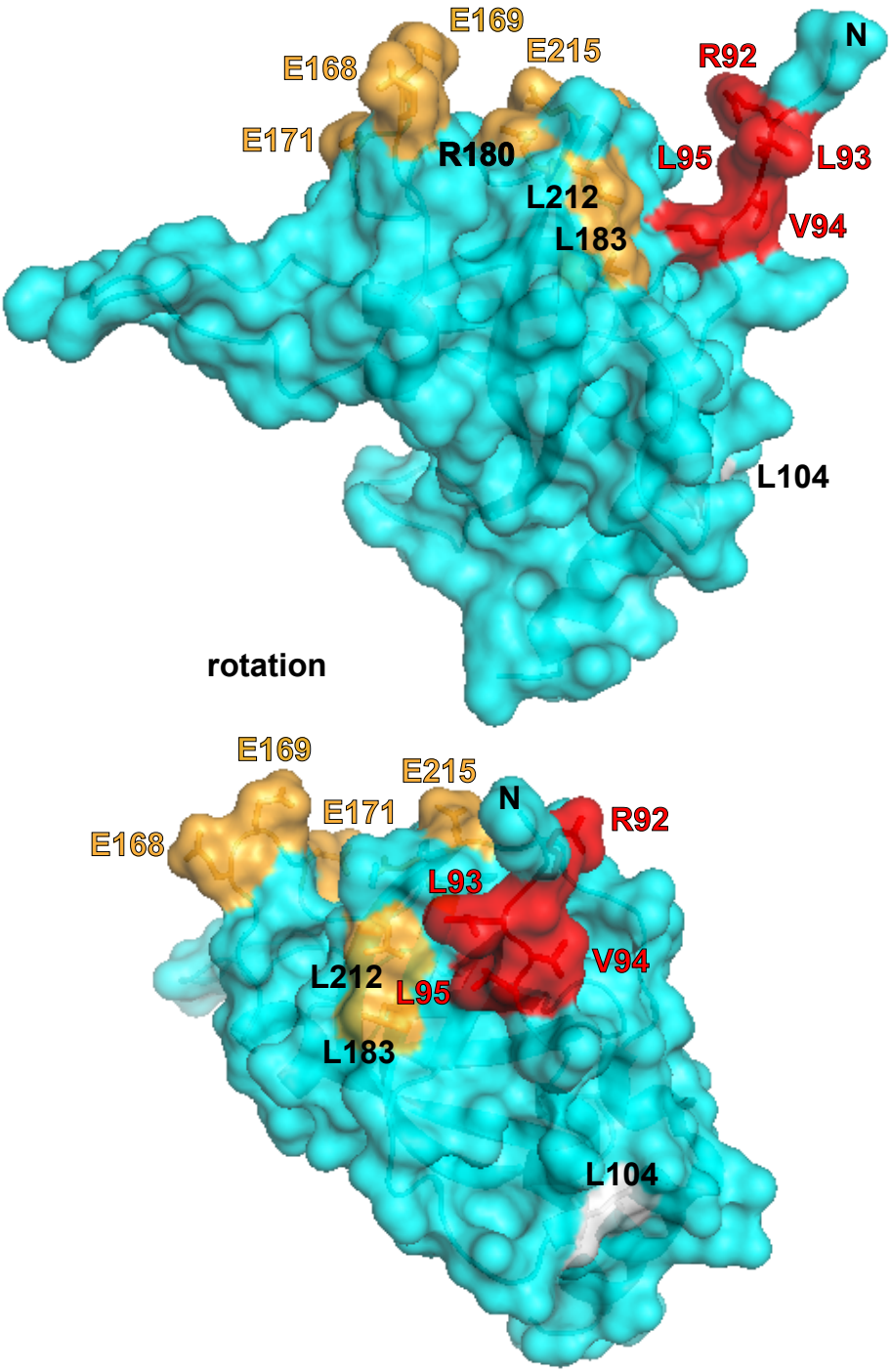

Figure S4. Relative locations of the TEL patch, NOB, and L104 regions on the surface of the TPP1 OB domain, Related to Figures 1 and 4. Two separate surface views of TPP1 OB with TEL patch residues shown in mustard, NOB residues in red, and L104 in grey.

SUPPLEMENTARY EXPERIMENTAL PROCEDURES

Plasmid constructs and mutagenesis: The following parental constructs used in this study have been described elsewhere: pFBHTb-Smt3star-hPOT1 for purification of insect cell-expressed human POT1 (Kocak et al., 2014); pET-Smt3-TPP1-N WT and L104A for bacterial expression of TPP1-N (aa 90-334) (Kocak et al., 2014; Nandakumar et al., 2012; Wang et al., 2007); pET-Smt3 vector for bacterial expression of constructs newly described in this study (MTA with Cornell University) (Mossessova and Lima, 2000); pTERT-cDNA6/myc-HisC and phTR-BluescriptIISK(+) constructs for overexpression of telomerase in HEK 293Tcells (Nandakumar et al., 2012); pTet-IRES-eGFP-BI4 vector, p3x-FLAG-TPP1-BI4 plasmid for Tet-inducible expression of FLAG-tagged human TPP1 (aa 87-544) in HeLa-EM2-11ht cells, and pd1gfpPtetmiR vector for Flp recombinase-mediated stable clone generation (MTA with Tet System Holdings GmbH & Co KG) (Nandakumar et al., 2012).

For expression of N-terminal 3X-FLAG-tagged mTERT in human cell lines, we substituted the mTERT cDNA sequence (pCiteE-mTERT plasmid was a kind gift from Julian Chen, Arizona State University) for the human TERT cDNA sequence in pTERT-cDNA6/myc-HisC using Gibson Assembly (New England Biolabs; NEB).

3X-FLAG-tagged TPP1 ΔNOB and L104A were cloned into the pTet-IRES-eGFP-BI4 and p3X-FLAG-TPP1-F3 vectors as described previously (Nandakumar et al., 2012). Myc-tagged POT1 and TIN2 were similarly amplified from plasmids containing the respective cDNA sequences (Kocak et al., 2014; Nandakumar et al., 2012) and cloned into the pTet-IRES-eGFP-BI4 vector to furnish p6X-Myc-POT1-BI4 and p6X-Myc-TIN2-BI4, respectively.

For bacterial expression of TPP1-N variants ΔNOB, 92-95A, 92-93A, 94-95A, and mNOB, appropriate TPP1-N sequences were cloned into the in pET-Smt3 vector using standard restriction endonuclease-mediated cloning. TPP1-N variants 96A and 100-101A were generated by QuikChange site-directed mutagenesis (Agilent technologies) using pET-Smt3-TPP1-N WT as template.

The construct pET-Smt3-hOB-hDBD was created for expression of hOB-hDBD WT, which consists of the OB domain of TPP1 (aa 88-250) and the DNA binding domain (DBD) of human POT1 (aa 2-303), linked by a 29 aa glycine and serine-rich linker NH_2-VDGSGGSSGSGGSGSSGSSGGSKLAAALD-COOH. This was established by

first splitting the multiple cloning site of the pET-Smt3 vector by inserting the cDNA sequence coding for the glycine-serine stretch (IDT) between the *SalI* and *HindIII* restriction sites. The human OB domain was cloned between the upstream *BamHI* and *SalI* sites, while the DBD was cloned between the downstream *HindIII* and *XhoI* sites. A similar strategy was used to create the mOB-hDBD and the hNOB/mOB-hDBD constructs (the N-termini of these proteins are specified in Fig. S3A). hOB-hDBD mutants (ΔNOB, 92-95A, and EE-AA) were generated by QuikChange site-directed mutagenesis (Agilent technologies) using hOB-hDBD WT as template.

For insect cell expression of TPP1-N we engineered a pFBHTb-sumostar-TPP1-N plasmid using the strategy described for engineering $(His)_6$-SUMOstar human POT1 (Kocak et al., 2014).

All oligonucleotides used in this study were purchased from IDT.

Purification of protein expressed in insect cells: Full-length human POT1 was expressed as a SUMOstar-$(His)_6$-POT1 fusion protein in baculovirus-infected High Five cells (Thermo Fisher Scientific), as described previously (Kocak et al., 2014). Briefly, POT1 was purified from the soluble cellular lysate with Ni-NTA agarose resin (Qiagen). After tag cleavage with SUMOstar protease (LifeSensors), untagged protein further purified by Superdex 200 size-exclusion chromatography (GE Healthcare Life Sciences) in 25 mM Tris-Cl (pH 8), 150 mM NaCl, and 2 mM DTT. The POT1-TPP1-N heterodimeric complex was similarly prepared from insect cells co-infected with viruses separately expressing $(His)_6$-SUMOstar-POT1 and $(His)_6$-SUMOstar-TPP1-N fusion proteins. Typical final yields were 2 and 6 mg per liter of culture for POT1 and the POT1-TPP1-N heterodimer, respectively.

Purification of protein expressed in bacteria: WT and variants of TPP1-N and OB-hDBD were expressed in *E. coli* BL21(DE3) strain as Sumo-$(His)_{10}$-fusion proteins. For protein purification, cells were harvested, sonicated, and centrifuged to clarify the soluble cellular lysates. Fusion proteins were purified with Ni-NTA agarose resin (Qiagen) and eluted with buffer containing 300 mM imidazole. Following tag cleavage with Ulp1 protease (MTA with Cornell University) (Mossessova and Lima, 2000) TPP1-N or OB-hDBD was further purified by Superdex 75 size-exclusion chromatography (GE Healthcare Life Sciences) in 25 mM Tris-Cl (pH 8), 100 mM NaCl, and 2 mM DTT. Typical final yields were 2 mg and 1-2 mg per liter of culture for TPP1-N and the OB-DBD constructs, respectively.

Primer extension assay: Super telomerase extracts were prepared from HEK 293T cells transiently transfected with constructs to express hTR and 3X-FLAG-tagged hTERT (or 3X-FLAG-tagged mTERT), as previously described (Cristofari and Lingner, 2006). Extension assays (Blackburn et al., 1989) supplemented with α^{32}P-dGTP were performed for an hour at approximately 30ºC and included super telomerase extract, 1 μM primer a5 [5'-TTAGGGTTAGCGTTAGGG-3'; (Wang et al., 2007)] and 500 nM of the purified TPP1-N variants, POT1 or OB-hDBD chimeras following a previously detailed method (Nandakumar et al., 2012). Extension products were precipitated with ethanol, dissolved in formamide loading dye and resolved on a 10% polyacrylamide/ 7 M urea/ 1x TBE sequencing gel. The data were imaged using a Phosphorimager (Storm; GE Healthcare Life Sciences) and analysis was performed with ImageQuant TL software (GE Healthcare Life Sciences) using 1D analysis and the rolling ball method for background correction. Activity was scored by quantitating the signal for the entire lane. Processivity values were obtained by dividing the total intensity from bands representing addition of 9 or more hexad repeats by the total intensity in the lane (omitting repeats 1 and 2) using the rolling ball method to define background.

HeLa culture and stable cell line generation: Tetracycline-inducible protein expression was performed in HeLa-EM2-11ht cells that constitutively express a tetracycline-controlled transcriptional activator and contain a thymidine kinase gene that can be excised with Flp recombinase for facilitating cassette exchange (Nandakumar et al., 2012; Weidenfeld et al., 2009). HeLa-EM2-11ht cells were cultured at 37°C in the presence of 5% CO_2 and propagated in modified DMEM (Dulbecco's Modified Eagle Medium; Gibco 11995-065) medium containing 100 U/mL penicillin, 100 μg/mL streptomycin, and 10% fetal bovine serum. Stable clones for doxycycline-inducible expression of TPP1 (ΔNOB and L104A) were engineered by the same procedure used to create the TPP1 WT line (Nandakumar et al., 2012). Briefly, cells were co-transfected with Lipofectamine 2000 (Thermo Fisher Scientific) and 1 ug each of the p3X-FLAG-TPP1-F3 (TPP1ΔNOB or TPP1-L104A) and a Flp recombinase-expressing plasmid also encoding puromycin resistance. One day of positive selection was performed with puromycin (5 ug/mL; Sigma-Aldrich), followed by 10 days of negative selection in fresh medium adjusted to 50 μM ganciclovir (Sigma-Aldrich). Individual clones were picked and expanded, and two positive clones of each TPP1 variant were selected based on GFP fluorescence (From IRES-GFP locus downstream of TPP1 construct) and Western blot analysis of FLAG-

TPP1 signal after overnight induction with doxycycline (200 ng/mL). Protein expression of POT1, TIN2, and TPP1 from transiently transfected p6X-Myc-POT1-BI4 and p6X-Myc-TIN2-BI4 plasmids and from the stable cell lines expressing FLAG-TPP1 (WT, ΔNOB, and L104A) were induced with doxycycline (200 ng/mL).

Co-immunoprecipitation: HeLa-EM2-11ht cells were transfected with 1 ug each of plasmids containing FLAG-TPP1 WT, FLAG-TPP1 ΔNOB, Myc-POT1, or Myc-TIN2 plasmid. 48 h after transfection/induction with doxycycline, cells were washed with PBS, trypsinized, and dislodged with medium containing 50% fetal bovine serum to inactivate the trypsin. Cell pellets were resuspended in 400 µL of lysis buffer [50 mM Tris-Cl (pH 7.4), 20% glycerol, 1 mM EDTA, 150 mM NaCl, 0.5% Triton X-100, 0.02% SDS, 1 mM dithiothreitol, 2 mM phenylmethylsulfonyl fluoride, and complete protease inhibitor cocktail (Roche)] and kept on ice. Next, 33 µL of 4 M NaCl was added followed by 433 µL of water before centrifuging at 16,000 x g for 10 min. Supernatants were used directly in immunoprecipitation. A portion of the lysate (50 µL) was kept aside to serve as an "input" sample. 30 µL of pre-washed anti-FLAG M2 affinity beads slurry (Sigma; A2220) was added to the remaining supernatant and the samples were rocked overnight at 4°C. The beads were washed three times with 0.5X lysis buffer and the bound proteins were eluted in 60 µL of 2X SDS gel loading buffer. All samples were heated for 10 min at 95°C and analyzed by SDS-PAGE followed by immunoblotting with HRP-conjugated anti-FLAG or anti-myc antibodies.

Immunoblotting: Proteins from cellular lysates or immunoprecipitation were resolved by SDS-PAGE, transferred to nitrocellulose (BioRad), and blocked with StartingBlock (TBS) blocking buffer (Thermo Scientific). Immunoblotting was performed following standard procedures and 1:10,000 dilution of the following antibodies: mouse monoclonal anti-FLAG M2-HRP conjugate (Sigma; A8592), mouse monoclonal anti-c-Myc (Developmental Studies Hybridoma Bank; 9E10) HRP conjugate (Santa Cruz; sc-40 HRP), and mouse monoclonal anti-β-actin antibody (Sigma; A5441) in conjunction with secondary horseradish peroxidase-conjugated goat antibody against mouse IgG (Santa Cruz Biotechnology). Antibodies were detected by chemiluminescence with ECL plus reagents (Pierce ECL Western Blotting Substrate; Thermo Scientific). The data were visualized using a gel-documentation system (ChemiDoc™ MP System; BioRad). Quantitation of actin or FLAG band intensity was performed using ImageJ software.

Immunofluorescence (IF) and fluorescence in situ *hybridization (FISH) microscopy:* Stable cell lines expressing either TPP1 WT, ΔNOB, or L104A were induced with doxycycline for 3 days and then ~100,000 cells were seeded on coverslips in a 12 well plate with growth medium containing doxycycline. Twenty-four hours post-seeding the medium was removed and the cells were washed with PBS. All subsequent steps were performed at room temperature. Cells were fixed with 4% formaldehyde in PBS for 10 min and washed three times for 5 min in PBS before permeabilization in PBS containing 0.5% Triton-X 100 for 10 min. IF-FISH experiments for telomerase recruitment were performed as described previously (Nandakumar et al., 2012). Briefly, IF was first performed to visualize FLAG-TPP1 proteins using mouse monoclonal anti-FLAG M2 (Sigma; F1804; 1:500) in combination with Alexa Fluor 568-conjugated anti-mouse IgG (Life Technologies). Subsequently a mixture of Cy5-conjugated probes complementary to TR was used at a concentration of 30 ng per probe per coverslip to detect TR by FISH (Abreu et al., 2010). The cells were washed three times in PBS and mounted on microscope slides using ProLong Gold mounting medium with DAPI (Life Technologies). Coverslips were sealed with transparent nail polish and stored at -20°C until the time of imaging. A laser scanning confocal microscope (SP5; Leica, Germany) equipped with a 100x oil objective was used to image IF-FISH experiments. The images were processed with ImageJ and Adobe Photoshop, and colocalizations were quantified manually by two separate individuals.

Telomere restriction fragment length analysis: Genomic DNA was purified by the GenElute kit (Sigma, G1N350-1KT) from stable cell lines overexpressing either FLAG-TPP1 constructs or a vector control. DNA (2 µg) was digested with *HinfI* and *RsaI* and incubated overnight at 37°C. The digested DNA was run on a 25 cm long 0.8% agarose-1X TBE gel along with a lambda DNA-HindIII digest ladder (NEB) at a constant 50 V for 21-23 h. The gel was imaged with a fluorescent ruler and then dried at 55°C for one hour prior to denaturation in 0.5 M NaOH for 30 min. The gel was then rinsed with water, neutralized with 1.5 M NaCl and 0.5 M Tris-Cl (pH 7.5) for 30 min, and prehybridized in Church buffer [0.5 M sodium phosphate buffer (pH 7.2), 1% bovine serum albumin, 1 mM EDTA, and 7% SDS] for 30 min at 65°C in a rotating hybridization oven. T4 polynucleotide kinase was used to 5' ^{32}P-label a $(TTAGGG)_4$ oligonucleotide, which was added at 20 million cpm to the gel. Hybridization was continued overnight at 55°C. The gel was then washed three times with 2X SSC for 10 min at 55°C and exposed to a phophorimager screen. The gel was analyzed using the Imagequant TL software and calibrated using the molecular

weights of the lambda DNA-*HindIII* digest ladder. The mean telomere length for each lane was plotted as a function of days in culture for each cell line.

Telomere localization of TPP1 constructs: Telomeres were visualized by fluorescence *in situ* hybridization (FISH) using a fluorescent telomeric PNA probe. Briefly, cells were fixed for 10 min with 4% formaldehyde in PBS, washed, then permeablized for 10 min in PBS containing 0.5% Triton X-100. Cells were then washed twice in PBS and soaked in 2X SSC, 50% formamide for 5 min. 40 μl of hybridization solution containing 0.3 μg/ml Cy3-conjugated PNA-$(CCCTAA)_3$ probe was placed on a microscope slide, and a coverslip containing cells from each engineered stable cell line (WT, ΔNOB, L104A) was inverted on the hybridization solution. DNA was denatured by heat for 6 min at 80°C followed by hybridization for two hours at room temperature. After hybridization the slides were washed twice at room temperature with 50% formamide in 2X SSC for 30 min. Slides were then washed with PBS and used for subsequent immunofluorescence (IF). IF was performed to visualize FLAG-TPP1 constructs to determine telomere localization. For IF, cells were blocked for 30 min with 1 mg/ml BSA, 3% goat serum, 0.1% Triton X-100, and 1 mM EDTA (pH 8.0) in PBS. FLAG-TPP1 constructs were visualized using mouse monoclonal anti-FLAG M2 (Sigma; F1804; 1:500) in combination with Alexa Fluor 633-conjugated anti-mouse IgG (Life Technologies; A21052). Cells were washed three times with PBS and mounted on microscope slides using ProLong Gold mounting medium with DAPI (Life Technologies). Imaging and analysis was performed as described above.

SUPPLEMENTARY REFERENCES

Abreu, E., Aritonovska, E., Reichenbach, P., Cristofari, G., Culp, B., Terns, R.M., Lingner, J., and Terns, M.P. (2010). TIN2-tethered TPP1 recruits human telomerase to telomeres in vivo. Mol Cell Biol *30*, 2971-2982.

Blackburn, E.H., Greider, C.W., Henderson, E., Lee, M.S., Shampay, J., and Shippen-Lentz, D. (1989). Recognition and elongation of telomeres by telomerase. Genome *31*, 553-560.

Chen, J.L., and Greider, C.W. (2003). Determinants in mammalian telomerase RNA that mediate enzyme processivity and cross-species incompatibility. EMBO J *22*, 304-314.

Cristofari, G., and Lingner, J. (2006). Telomere length homeostasis requires that telomerase levels are limiting. EMBO J *25*, 565-574.

Gillis, A.J., Schuller, A.P., and Skordalakes, E. (2008). Structure of the Tribolium castaneum telomerase catalytic subunit TERT. Nature *455*, 633-637.

Kocak, H., Ballew, B.J., Bisht, K., Eggebeen, R., Hicks, B.D., Suman, S., O'Neil, A., Giri, N., Maillard, I., Alter, B.P.*, et al.* (2014). Hoyeraal-Hreidarsson syndrome caused by a germline mutation in the TEL patch of the telomere protein TPP1. Genes Dev *28*, 2090-2102.

Mossessova, E., and Lima, C.D. (2000). Ulp1-SUMO crystal structure and genetic analysis reveal conserved interactions and a regulatory element essential for cell growth in yeast. Mol Cell *5*, 865-876.

Nandakumar, J., Bell, C.F., Weidenfeld, I., Zaug, A.J., Leinwand, L.A., and Cech, T.R. (2012). The TEL patch of telomere protein TPP1 mediates telomerase recruitment and processivity. Nature *492*, 285-289.

Wang, F., Podell, E.R., Zaug, A.J., Yang, Y., Baciu, P., Cech, T.R., and Lei, M. (2007). The POT1-TPP1 telomere complex is a telomerase processivity factor. Nature *445*, 506-510.

Wang, Y., and Feigon, J. (2017). Structural biology of telomerase and its interaction at telomeres. Curr Opin Struct Biol *47*, 77-87.

Weidenfeld, I., Gossen, M., Löw, R., Kentner, D., Berger, S., Görlich, D., Bartsch, D., Bujard, H., and Schönig, K. (2009). Inducible expression of coding and inhibitory RNAs from retargetable genomic loci. Nucleic Acids Res *37*, e50.

Zaug, A.J., Podell, E.R., Nandakumar, J., and Cech, T.R. (2010). Functional interaction between telomere protein TPP1 and telomerase. Genes Dev *24*, 613-622.